IEEE Open Journal of
Power Electronics

Received 12 September 2023; accepted 11 October 2023. Date of publication 16 October 2023;
date of current version 26 October 2023. The review of this paper was arranged by Associate Editor Ui-Min Choi.

Digital Object Identifier 10.1109/OJPEL.2023.3324989

Improved Robust LQR Digital Control Method for High Bandwidth Inverters With Time Delay and Uncertain Parameters

JICHAO NING [1], HONGQI BEN [2], XUESONG WANG [3], AND TAO MENG [4] (Member, IEEE)

[1]Harbin Institute of Technology, Harbin 150001, China
[2]School of Electrical Engineering and Automation, Harbin Institute of Technology, Harbin 150001, China
[3]State Grid Harbin Power Supply Company, Harbin 150001, China
[4]School of Mechanical and Electrical Engineering, Heilongjiang University, Harbin 150080, China

CORRESPONDING AUTHOR: JICHAO NING (e-mail: 18b906005@stu.hit.edu.cn)

ABSTRACT A feedforward combined with state feedback linear quadratic regulator (LQR) is proposed to reduce the output waveform distortion and load regulation of high-bandwidth inverters. However, when digital control is adopted, the additional delays introduced by each part can lead to unmodeled model errors, which not only seriously affects the stability of the system, but also complicates the design of the controller. Therefore, a method of converting the design of a digital control system into time domain pole position selection is proposed to simplify the analysis and design of the controller, and can easily convert the time domain control method into the corresponding digital control. Furthermore, to ensure system stability in the presence of parametric uncertainties in the filter components and input bus voltage, robustness to parametric uncertainties is incorporated into the proposed digital control method. The feasibility, effectiveness and superiority of this method were verified through simulation comparison and experiments.

INDEX TERMS Delay stability, parameter uncertainty, inverter, LQR digital control, robustness, asymmetric sine wave.

I. INTRODUCTION

High-bandwidth inverters are widely used in electric vehicle powertrains, photovoltaic energy storage systems, and special power supplies. Microarc oxidation can greatly enhance the corrosion resistance, wear resistance, and other properties of nonferrous metals, and is therefore widely used in industrial, medical, and aerospace fields [1], [2]. The current microarc oxidation power supply usually adopts an asymmetrical rectangular pulse waveform, and the capacitive characteristics of the load can cause transistor voltage and current spikes [3]. This can increase the electrical stress on the transistor which in turn can reduce the reliability of the device.

Therefore, an asymmetric sinusoidal output waveform as shown in Fig. 1, has been proposed, which requires a wide range of adjustable output frequencies and amplitudes of positive and negative half-cycles. Since the asymmetric sine wave contains rich harmonics and the output waveform frequency is high (usually 1 kHz or above), the inverter must have high bandwidth and control performance, which entails higher requirements for the control system. PI control is easy to implement and can ensure stability at will, but it is usually difficult to achieve such a high bandwidth and the load regulation rate is also difficult to guarantee. To improve the control performance of the inverter, many control methods such as proportional resonance (PR) control, deadbeat control, repetitive control, sliding mode control (SMC) and model predictive

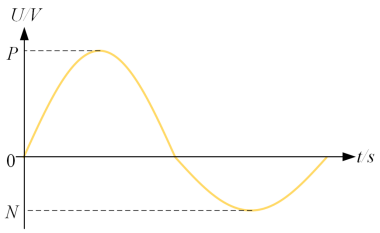

FIGURE 1. Schematic diagram of an asymmetric sine wave.

control (MPC) [4], [5], [6], [7], [8], [9] are widely used and studied.

These methods have achieved good results for conventional sine wave inverters, but are not suitable for asymmetric sine wave inverters. PR and repetition control can effectively eliminate harmonics to achieve higher sine wave quality. However, asymmetric sine waves should ensure harmonic amplitude and phase as much as possible, and frequency adjustment is not conducive to the realization of PR control and repetition control. SMC has high robustness to disturbances and a fast dynamic response. However, the nonsmooth asymmetric sinusoidal nature makes it difficult for SMC to maintain high waveform quality. Due to the high frequency of the output waveform, MPC requires a very low control cycle to achieve high waveform quality, and the microprocessor cannot bear this computing demand. Compared with these methods, the method based on state feedback proposed in [10], [11], [12], [13] can arbitrarily modify the closed-loop poles, which can better improve the control performance at a fixed switching frequency, so it has the potential to solve the control problems encountered by asymmetric sinusoidal inverters. In particular, the control signal of the switching converter control system needs to be modulated to generate a duty cycle to control the transistor, and the duty cycle is limited so that the control signal is also limited. The linear quadratic regulator (LQR) can ensure that the controlled signal tracks the reference as much as possible when the control signal is limited [14], which is especially suitable for asymmetric sine wave inverters.

Modern control systems are usually implemented using digital controllers, and many parts, such as sampling and digital modulation introduce additional delays. When the switching frequency is low, the extra delay is much smaller than the control period, and has little impact on the system. Therefore, the method commonly used by authors in [15], [16] to design digital LQR controllers based on the system discrete model using the MATLAB dlqr function is effective. As the switching frequency increases, the control period shortens, and the proportion of the additional delay to the control period increases. The influence of the unmodeled characteristics of the system caused by the delay is more serious, making the stability of the actual system more dependent on the actual tuning of the matrices Q and R, which is very inconvenient.

The impact of delay is also reflected in other fields of power electronics, such as the current control stability of a typical grid-connected inverter with an LCL filter [17]. To solve the effect of delay, it is effective to apply the well-known Smith predictor [18], state observer [19] and deadbeat control [20]. However, these methods are highly dependent on model accuracy, and the delay will cause unmodeled characteristics of the model. The time-varying duty cycle can cause varying delays, so the effect is limited in the case of high bandwidth. The linear extrapolation approach [21] is model-independent, but also has limited compensation at high frequencies. Different modulation strategies [22], [23] have also been proposed to reduce the delay caused by the modulation part, but the delay has not disappeared and will still affect the system stability. Another simple method is to sample close to the control update point to reduce the delay [24], but this will introduce more noise, and not sampling at the midpoint will also cause errors in the average current sampling, further causing model errors. In addition, this method cannot reduce the delay introduced by the sensor itself. The delay can also be compensated by using a phase lead of a second-order generalized integrator (SOGI) at the resonant frequency [25], [26]. Dead time compensation controllers [27], [28] can also be used to compensate for delay; however, this approach becomes quite complex when state feedback control is used. The method of linear matrix inequality (LMI) combined with the Lyapunov-Krasovskii functional is an effective and widely used method for analyzing the stability of state feedback systems with time delays [29], [30], [31], [32]. However, when designing a time-delay stable controller using the LMI method, nonlinear terms will be introduced, which greatly complicates the design of the controller. The study in [33] proposes a method for correlating continuous and discrete systems through delays, which is beneficial for analyzing and designing the stability of digital control systems.

In addition, a high bandwidth will make the system more sensitive to parametric uncertainties from changes in inductance values with current, manufacturing-induced tolerances in capacitance values, and bus voltage fluctuations. Uncertain parameters also make methods based on accurate models such as deadbeat difficult to ensure stability. For single-parameter uncertainty, methods such as the use of resonant controllers [34] and active damping [35] are applied to stabilize the system. For multiparameter uncertainty, methods such as adaptive control [36], [37], LMI methods [38], [39], [14] and H∞ control [40], [41], [42] have been proposed to stabilize the system. However, considering the robustness to parameter uncertainty in digital control systems is still relatively difficult, and there is no convenient method.

Aiming at the above problems, this article first proposes a state feedback control structure with feedforward, then gives the stability criteria of the digital control system with delay, and transforms the design of the digital controller into the pole configuration of the continuous system. Based on this, a robust LQR digital controller is designed.

The main contributions and advantages of this article are as follows:

1) A state feedback controller with feedforward is proposed. Different from the method of introducing error integral feedback in [14], [15], the proposed method controls the waveform envelope through the feedforward signal and controls the error through the state feedback. Therefore, this method does not require a high-gain controller, is less sensitive to delay, and has better stability, waveform quality, and load regulation.
2) The method also considers the stability and design method of digital controllers with additional delays not considered in [14], [15], [43], [44] and replaces the complex Lyapunov- Lyapunov-Krasovskii functional method by converting the design of a digital controller

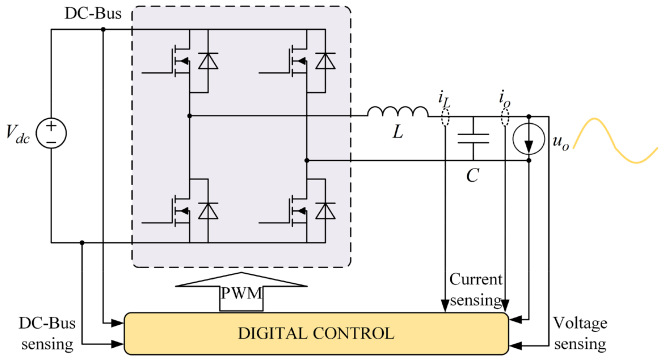

FIGURE 2. Schematic diagram of an asymmetric sine wave inverter.

with time delays into the pole configuration of a continuous system. This not only organically combines the digital system and the continuous system so that the existing time-domain control methods such as LQR and robust control can also be easily converted to digital control, but also greatly simplifies the design of the digital control system.

3) No actual parameter tuning is needed, the stability is predictable, and it has excellent control effect, and it is convenient for engineering applications.

The remainder of the article is organized as follows: In Section II, the system model and the structure of the controller are established, the effect of delay on the stability of the digital control system is then investigated, and the stability criterion is given. In Section III, the stability criterion of a digital control system with delay is translated into a pole configuration problem, which leads to the design of a robust LQR digital controller. Design examples, detailed comparisons of effects with existing methods and experimental verification are presented in Section IV. Finally, Section V concludes the article. When the negative half cycle of the asymmetric sine wave is zero, the harmonic components contained are the most complex, so the simulation and experiments in this article are based on the asymmetric sine half wave.

II. ANALYSIS OF THE STABILITY OF DIGITAL LQR CONTROL WITH DELAY

In this section, the system is first modeled, and the control structure is given. Then, an example is given to illustrate the possible instability of controllers designed by conventional digital LQR design methods (e.g., dlqr) in inverter digital control systems with delay due to unmodeled system characteristics. Finally, a simple stability criterion for digital control systems with delay is proposed.

A. SYSTEM MODELING AND CONTROLLER STRUCTURE

Compared with controlling the integral of the error, full utilization of the system's information can achieve better control performance.

The state equation for the full-bridge inverter shown in Fig. 2 with bipolar modulation can be expressed as:

$$\begin{cases} L\frac{di_L(t)}{dt} = -u_c(t) + 2V_{dc}u(t) - V_{dc} \\ C\frac{du_c(t)}{dt} = i_L(t) - i_o(t) \\ u_o(t) = u_c(t) \end{cases} \tag{1}$$

where u denotes the control signal, u_c is the capacitor voltage (i.e., output voltage u_o), i_L is the inductor current, and V_{dc} is the DC bus voltage. In matrix form, (1) can be expressed as:

$$\begin{aligned} \begin{bmatrix} \dot{i_L}(t) \\ \dot{u_c}(t) \end{bmatrix} &= \begin{bmatrix} 0 & -\frac{1}{L} \\ \frac{1}{C} & 0 \end{bmatrix} \begin{bmatrix} i_L(t) \\ u_c(t) \end{bmatrix} + \begin{bmatrix} \frac{2V_{dc}}{L} \\ 0 \end{bmatrix} u(t) \\ &\quad - \begin{bmatrix} 0 \\ \frac{1}{C} \end{bmatrix} i_o(t) - \begin{bmatrix} \frac{V_{dc}}{L} \\ 0 \end{bmatrix} \\ u_o(t) &= \begin{bmatrix} 0 & 1 \end{bmatrix} \begin{bmatrix} i_L(t) \\ u_c(t) \end{bmatrix} \end{aligned} \tag{2}$$

After calculation, the equilibrium point of the state variable u_c in (2) is not the reference voltage u_{ref}, which means that the output of the system cannot always follow the reference signal by relying on state feedback alone. Therefore, a feedforward signal is added to the control signal to change the system equilibrium position as follows:

$$u(t) = \begin{bmatrix} k_1 & k_2 \end{bmatrix} \begin{bmatrix} i_L(t) \\ u_c(t) \end{bmatrix} + u_f(t) \tag{3}$$

where u_f is the feedforward signal used to move the equilibrium point of the system to the reference command and k_1, k_2 are the control gain. Since the output waveform frequency is much smaller than the switching frequency, neglecting the differential of the reference signal, the state variables of the system at the steady-state point satisfy the following relationship:

$$\dot{i_L}(t) = 0, \dot{u_c}(t) = 0, u_c(t) = u_{ref}(t) \tag{4}$$

Combining (2) to (4), the proposed control method can be obtained as follows:

$$\begin{aligned} u(t) = &\begin{bmatrix} k_1 & k_2 \end{bmatrix} \begin{bmatrix} i_L(t) \\ u_c(t) \end{bmatrix} - \begin{bmatrix} k_1 & k_2 \end{bmatrix} \begin{bmatrix} i_o(t) \\ u_{ref}(t) \end{bmatrix} + \frac{1}{2} \\ &+ \frac{u_{ref}(t)}{2V_{dc}} \end{aligned} \tag{5}$$

Through the action of the feedforward signal, as long as the system is stable, the equilibrium position of the system will naturally become $i_L = i_o$, $u_c = u_{ref}$. When the controller shown in (5) is used, system (2) can be expressed as follows:

$$\begin{aligned} \begin{bmatrix} \dot{i_L}(t) \\ \dot{u_c}(t) \end{bmatrix} &= A_c \begin{bmatrix} i_L(t) \\ u_c(t) \end{bmatrix} + E_c i_o(t) + F_c u_{ref} \\ u_o(t) &= C_c \begin{bmatrix} i_L(t) \\ u_c(t) \end{bmatrix} \end{aligned} \tag{6}$$

where $A_c = \begin{bmatrix} 2k_1V_{dc}/L & (2k_2V_{dc}-1)/L \\ 1/C & 0 \end{bmatrix}$, $E_c = \begin{bmatrix} -2k_1V_{dc}/L & -1/C \end{bmatrix}^T$, $F_c = \begin{bmatrix} (1-2k_2V_{dc})/L & 0 \end{bmatrix}^T$ and $C_c = \begin{bmatrix} 0 & 1 \end{bmatrix}$. According to (6), the expression of the transfer function of u_o can be derived as follows:

$$\begin{aligned} u_o(s) &= Z_o(s)\, i_o(s) + G_p(s)\, u_{ref}(s) \\ &= C_c(sI - A_c)^{-1}\left(E_c i_o(s) + F_c u_{ref}(s)\right) \\ &= \left(-Lsi_o(s) + (1-2k_2V_{dc})\, u_{ref}(s)\right)/D(s) \end{aligned} \tag{7}$$

where

$$\begin{aligned} D(s) &= LCs^2 - 2k_1V_{dc}Cs + (1-2k_2V_{dc}) = LC\,|sI - A_c| \\ Z_o(s) &= \frac{-Ls}{LCs^2 - 2k_1V_{dc}Cs + (1-2k_2V_{dc})} \\ G_p(s) &= \frac{(1-2k_2V_{dc})}{LCs^2 - 2k_1V_{dc}Cs + (1-2k_2V_{dc})} \end{aligned} \tag{8}$$

where $Z_o(s)$ represents the output impedance and $G_p(s)$ is the transfer function from the reference signal to the output voltage without considering the influence of the output current. As can be derived from (8), the numerator of the output impedance of the inverter is reduced to Ls when controller (5) with a feedforward signal is used. When the frequency is lower than the crossover frequency, the amplitude of $D(s)$ is $\langle D(s)\rangle \approx 1 + 2|k_2|V_{dc} \gg 1$. Therefore, within the output waveform and its main harmonic frequency range, the output impedance is much smaller than Ls, significantly improving load regulation. In addition, the u_o of the system can track u_{ref} due to $\lim_{s\to 0} G_p(s) = 1$ when the frequency is lower than the crossover frequency. Therefore, the inverter can output an asymmetrical sine wave by controlling u_{ref} to be an asymmetrical sine wave.

Since the denominators of $Z_o(s)$ and $G_p(s)$ are both $D(s)$, and the zero point of $D(s)$ is related to $|sI - A_c|$, the stability of the system is only determined by the matrix A_c. Therefore, when designing the controller and analyzing the stability, the system model can be simplified as follows:

$$\dot{x}(t) = Ax(t) + Bu(t) = Ax(t) + BKx(t) \tag{9}$$

where $x = \begin{bmatrix} i_L & u_c \end{bmatrix}^T$, $K = \begin{bmatrix} k_1 & k_2 \end{bmatrix}$, $A = \begin{bmatrix} 0 & -1/L \\ 1/C & 0 \end{bmatrix}$, $B = \begin{bmatrix} 2V_{dc}/L & 0 \end{bmatrix}^T$, and k_1 and k_2 are coefficients. The matrix K is critical to the stability of the system.

B. INFLUENCE OF DELAY ON THE STABILITY OF THE DIGITAL CONTROL SYSTEM

For the continuous system shown in (9), the discrete model of the system can be obtained by the zero-order hold on method as follows:

$$x(k+1) = A_d x(k) + B_d K_d x(k) \tag{10}$$

where $A_d = e^{AT_c}$, $B_d = \int_0^{T_c} e^{At}dtB$, and K_d are discrete forms of A, B, and K, respectively, T_c is the control period, and k is a discrete series. For the system whose parameters are shown in Table 1, if the weight matrices $Q = \begin{bmatrix} 10 & 0 \\ 0 & 10 \end{bmatrix}$ and $R = 10$ are selected and the control period is equal to the switching period, then the digital LQR control law K_d can be obtained as $[-0.276 \quad -0.077]$ by using the dlqr function of MATLAB.

When the feedback control law K_d is adopted, the magnitudes of the eigenvalues of system (10) are all less than 1, which satisfies the stability criterion. Fig. 3(a) shows the simulation waveform when the sampling delay (i.e., sensor delay) is not considered; the waveform quality of the output waveform is good, which proves that the designed control law is stable. However, when there is a delay of 1.7 μs in the sampling part, the output waveform in Fig. 3(b) shows that the system has begun to appear unstable. When the control

TABLE 1. Simulation Parameters

Parameters	Descriptions	Values	Units
V_{dc}	Input voltage	500	V
V_p	Positive output voltage	260	V
V_n	Negative output voltage	0	V
f_o	Output frequency	1000	Hz
C_o	Output capacitor	2	μF
L_f	Filter Inductance	900	μH
f_s	Switching frequency	200	kHz
t_{sensor}	Sensor delay	1.7	μs

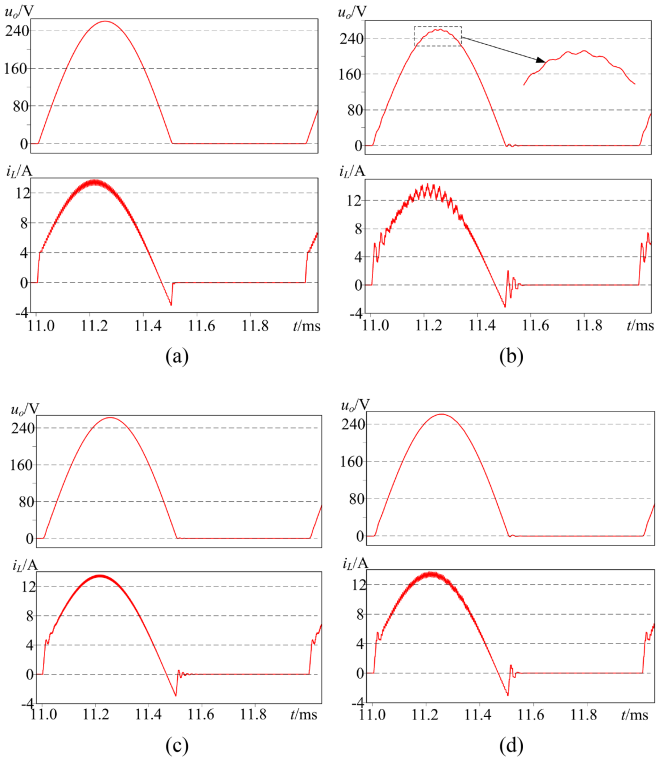

FIGURE 3. Output waveforms of the system using the digital controller designed by the dlqr method under different conditions. (a) $f_s = 200$ kHz, $t_{sensor} = 0$ μs. (b) $f_s = 200$ kHz, $t_{sensor} = 1.7$ μs. (c) $f_s = 300$ kHz, $t_{sensor} = 1.7$ μs. (d) $f_s = 200$ kHz, $t_{sensor} = 1.7$ μs, Q = 0.33I, R = 10.

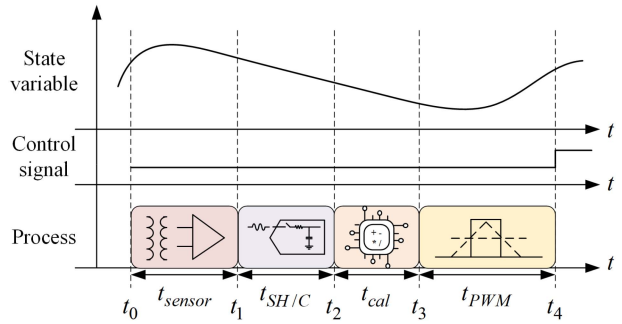

FIGURE 4. Schematic diagram of the processes from signal sensing to control signal generation.

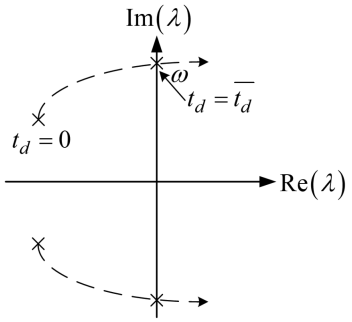

FIGURE 5. Schematic diagram of closed-loop pole variation with delay.

parameters and delay are consistent with those in Fig. 3(b) but the switching frequency becomes 300 kHz, the system is stable, and the output waveform is shown in Fig. 3(c). When the switching frequency and delay are consistent with those in Fig. 3(b) and the matrices $Q = \begin{bmatrix} 0.33 & 0 \\ 0 & 0.33 \end{bmatrix}$ and $R = 10$ are selected, the system is also stable, and the output waveform is as shown in Fig. 3(d).

It can be seen from Fig. 3 that the extra delay leads to unmodeled characteristics of the system, making typical digital controller design methods unable to guarantee the stability of the actual system. The effect of additional delay is rarely considered but cannot be ignored, which makes the stability of the inverter digital control system related to the weight matrices Q and R. Therefore, the actual control system needs to tune Q and R to make the system stable, which is very inconvenient for the stability analysis of the control system and the design of the controller. For this reason, an effective analysis and design method needs to be proposed.

C. STABILITY ANALYSIS OF THE DIGITAL CONTROL SYSTEM WITH DELAY

In an actual digital control system, state variables are detected by sensors and converted into digital signals by analog to digital convertors (ADCs). The digitalized signal is sent to a microprocessor for calculation, and a pulse width modulation (PWM) signal is generated. Completion of these processes, introduces a delay into the system. The actual digital control system, from sampling the state variables to changing the state variables via the control signal, is shown in Fig. 4. The sampling delay due to the sensor is denoted as t_{sensor}, $t_{SH/C}$ is the time required for ADC sample hold and conversion, t_{cal} is the time for the processor to perform data processing and control calculations, and t_{PWM} is the delay introduced by the digital PWM. As shown in Fig. 4, the state variables at t_0 are converted into control signals at t_4, causing a time delay of $t_4 - t_0$. This means that the changes in the state variables occurring at t_4 are actually caused by the control signals u generated based on the feedback state variables at t_0. Therefore, combined with the theory in [33], [45], the sufficient condition for stability of the digital control system with delay is that the feedback information at t_0 can be used to stabilize the system at t_4, which can be expressed as making the following system stable:

$$\dot{x}(t) = Ax(t) + BKx(t - t_d) \tag{11}$$

where $t_d = t_{sensor} + t_{SH/C} + t_{cal} + t_{PWM}$ represents the delay time from obtaining the feedback signal to the state variables being changed by the control signal.

Equation (11) relates the stability analysis and design of digital systems to that of continuous systems with delays so that the additional delay can be considered in the system model. This makes the stability of the digital control system no longer sensitive to the unmodeled characteristics caused by delay, and improves the robustness to delay. However, note that the system in (11) is not actually equivalent to the digital control system, and is only used for stability judgment and design.

The closed-loop pole locations of system (11) can be obtained by solving for λ of the following equation:

$$\left|\lambda I - A - BKe^{-\lambda t_d}\right| = 0 \tag{12}$$

Bringing the parameters into (12), the following can be obtained:

$$\left|\begin{bmatrix} \lambda & 0 \\ 0 & \lambda \end{bmatrix} - \begin{bmatrix} 0 & -1/L \\ 1/C & 0 \end{bmatrix} - e^{-t_d\lambda}\begin{bmatrix} 2V_{dc}/L \\ 0 \end{bmatrix}\begin{bmatrix} k_1 & k_2 \end{bmatrix}\right|$$
$$= LC\lambda^2 - 2V_{dc}e^{-t_d\lambda}(k_1C\lambda + k_2) + 1 = 0 \tag{13}$$

Based on solving (13), as the delay increases, the closed-loop pole of the system moves to the right half-plane of the complex plane, and the trajectory of the closed-loop pole position changing with the delay is shown in Fig. 5. This means that as the delay increases, the system stability decreases, causing a stable system to become unstable, which is consistent with the simulation results. The reverse is also true; therefore, as the switching frequency increases, the total delay decreases, and the system goes from unstable to stable. The critical point of the system stability is the closed-loop pole position located on the imaginary axis (i.e., $\lambda = j\omega$), which can be expressed as:

$$e^{-\lambda\overline{t_d}} = e^{-\omega j\overline{t_d}} = \cos\left(\omega\overline{t_d}\right) - j\sin\left(\omega\overline{t_d}\right) \tag{14}$$

where ω is the oscillation frequency of the system at critical stability and $\overline{t_d}$ is the maximum allowable delay for stability, which means that when $t_d = \overline{t_d}$, the closed-loop poles of the system (11) lie exactly on the imaginary axis.

Combining (13) and (14), the following can be obtained:

$$-LC\omega^2 - 2V_{dc}\left(\cos\left(\omega\overline{t_d}\right) - j\sin\left(\omega\overline{t_d}\right)\right)(k_1 C j\omega + k_2) + 1 = 0 \tag{15}$$

Equation (15) is equivalent to the fact that the real and imaginary parts of the equation are both zero, so the maximum allowable delay $\overline{t_d}$ for system stability and the corresponding oscillation frequency ω can be solved using the expressions:

$$\begin{cases} -LC\omega^2 - 2Ck_1V_{dc}\omega\sin\left(\overline{t_d}\omega\right) + 1 - 2k_2V_{dc}\cos\left(\overline{t_d}\omega\right) = 0 \\ -2Ck_1V_{dc}\omega\cos\left(\overline{t_d}\omega\right) + 2k_2V_{dc}\sin\left(\overline{t_d}\omega\right) = 0 \end{cases} \tag{16}$$

Equation (16) can be numerically solved by iteration or calculation software. According to the theory mentioned in Section 3.6 of [46], the criterion for system delay stability is

$$t_d < \overline{t_d} \tag{17}$$

When the stability condition of (17) is satisfied, that is, when the delay t_d of the system is less than the calculated maximum allowable delay $\overline{t_d}$, the time-delay system (11) is stable, and then, the corresponding digital control system is stable. Therefore, we can equivalently design a digital controller by designing a time-delay stable controller.

III. DESIGN OF A ROBUST LQR DIGITAL CONTROLLER

The design of the traditional delay stable controller needs to select the appropriate Lyapunov-Krasovskii functional first, and then transform it into the form of an LMI. Then it is converted into a form that can be used for controller design through matrix transformation. Finally, a solvable LMI form can be obtained through linearization. Not only is this not conducive to the design of the controller, but the conservatism and solvability depend on the selection of the Lyapunov-Krasovskii functional and the linearization method. Therefore, this section proposes a method to convert time-delay stability into a closed-loop pole position configuration, which effectively simplifies the design of time-delay stable controllers.

A. POLE POSITION CONFIGURATION DESIGN METHOD FOR A TIME-DELAY STABLE CONTROLLER

When $t_d = 0$, system (11) degenerates to (9); therefore, from Fig. 5, any stable closed-loop pole position of a delay-free system (9) corresponds to the maximum allowable delay $\overline{t_d}$ for a delay system (11). Therefore, if the closed-loop pole position corresponding to system (9) makes the $\overline{t_d}$ corresponding to system (11) satisfy $\overline{t_d} > t_d$, then system (11) must be stable. In this way, a closed region must be found on the complex plane. If the closed loop pole of system (9) is located in this region, system (11) must be stable.

The closed area that is easiest to describe is a semicircle. Therefore, first, the closed-loop poles of system (11) at $t_d = 0$

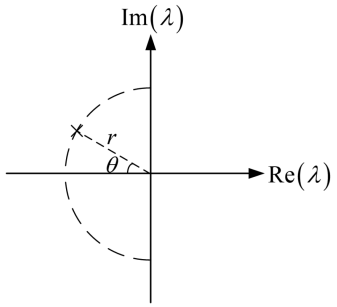

FIGURE 6. Location of the poles on the semicircular boundary.

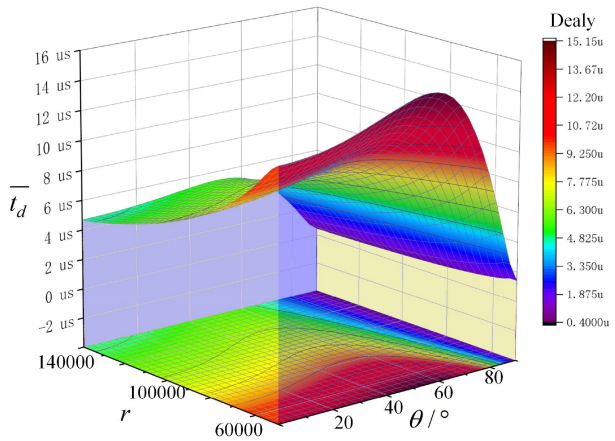

FIGURE 7. Maximum allowable delay for stabilization at different radii and angles.

are configured on a semicircular boundary, as shown in Fig. 6, and the poles can be expressed as follows:

$$p_{1,2} = -r\cos\theta \pm rj\sin\theta \tag{18}$$

Taking $\lambda = p_{1,2}$ as the solution of (13) at $t_d = 0$ into the equation, the corresponding feedback coefficient $k_{1,2}$ can be obtained by the corresponding coefficient method as follows:

$$k_1 = \frac{-rL\cos\theta}{V_{dc}},\ k_2 = \frac{\left(1 - r^2LC\right)}{2V_{dc}} \tag{19}$$

The following equation can be obtained by bringing (16) into (19):

$$\begin{cases} -LC\omega^2 - 2LCr\cos\theta\omega\sin\left(\overline{t_d}\omega\right) + r^2LC\cos\left(\overline{t_d}\omega\right) = 0 \\ 2LCr\cos\theta\omega\cos\left(\overline{t_d}\omega\right) + \left(1 - r^2LC\right)\sin\left(\overline{t_d}\omega\right) = 0 \end{cases} \tag{20}$$

where θ is the angle between the line from the pole to the origin and the real axis, and r is the radius of the semicircle.

By numerically solving (20), the relationship between all closed-loop pole positions located in the semicircle area and the corresponding maximum delay $\overline{t_d}$ can be obtained, as shown in Fig. 7. Fig. 7 demonstrates that when r is constant, the maximum allowable delay $\overline{t_d}$ will reach the maximum

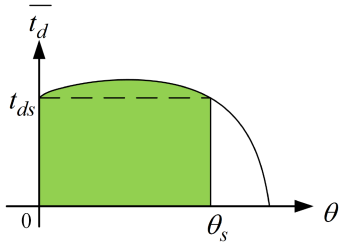

FIGURE 8. Delay stabilization region at radius r_s.

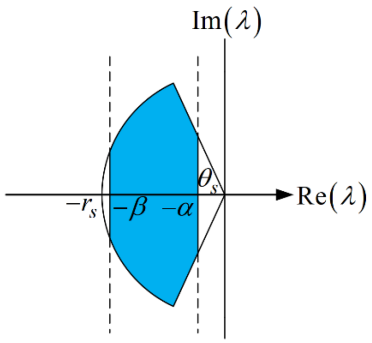

FIGURE 9. Closed-loop pole positions that satisfy the delay stability condition.

value at a certain angle, and then, as θ increases, the maximum allowable delay $\overline{t_d}$ of the system will decrease, and the stability of the system will worsen. Furthermore, according to the contour in Fig. 7, when the angle θ is constant, the maximum allowable delay $\overline{t_d}$ of the system monotonically increases with decreasing radius r. In LQR control, as the ratio of matrices Q and R increases, the designed closed-loop pole position becomes farther from the imaginary axis, so the $\overline{t_d}$ of the system is smaller, which explains why reducing the ratio of Q and R in the simulation can make an originally unstable system stable.

In addition, when the frequency of the output waveform increases, the system needs a higher bandwidth; that is, the closed-loop pole position of the system needs to be farther from the imaginary axis, which means that the system needs a shorter delay. For digital control systems, the delay introduced by sensors and calculations cannot be further reduced, so increasing the switching frequency is the easiest way to increase the system bandwidth and improve the quality of the output waveform.

A radius r_s is arbitrarily fixed in Fig. 7, and the cross-sectional view under this radius is drawn as shown in Fig. 8. The outline shown in Fig. 8 represents the maximum allowable delay $\overline{t_d}$ of the system corresponding to different θ under radius r_s. When $\theta = 0$, a $t_{ds} = \overline{t_d}(\theta = 0)$ can be obtained, where $\overline{t_d}(\theta = 0)$ represents $\overline{t_d}$ obtained when $\theta = 0$. At the same time, it must be possible to find a $\theta = \theta_s$ so that the maximum allowable delay $\overline{t_d}(\theta = \theta_s) = t_{ds}$ is obtained under this angle θ_s. In this way, a shaded area is enclosed in Fig. 8. In this shaded area, regardless of how the angle θ changes, it can be guaranteed that the corresponding maximum allowable delay $\overline{t_d}(\theta)$ is greater than t_{ds}. If $t_{ds} > t_d$, system (11) can be guaranteed to be stable in this shaded area.

When the angle is fixed, the upper limit of the maximum allowable delay $\overline{t_d}$ monotonically decreases with increasing radius r. Therefore, if a set (r_s, θ_s) can be found such that t_{ds} in this case is just greater than t_d, then the system can be stable under delay t_d for all $r < r_s$. In other words, for a system with time delay t_d, as long as the closed-loop pole position without time delay is within the fan-shaped area in Fig. 9, the system must be stable. In general, to meet the system dynamic performance requirements, the position of the closed-loop pole is usually limited, so the shaded part in Fig. 9 is finally selected as the configurable area of the closed-loop pole that meets the delay stability. where $Re(\lambda) = -\alpha$, β can be considered

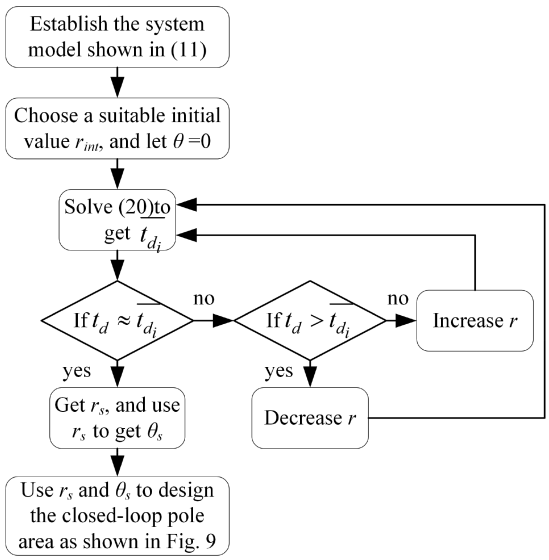

FIGURE 10. Flowchart for the design of a delay- stabilized closed-loop pole region.

optional rather than necessary. It is mainly used to limit the dynamic performance of the system and this limitation can be neglected by choosing $\alpha = 0$ and $\beta > r_s$.

In this way, the design of the digital controller is transformed into the controller design of the delay continuous system and then transformed into the closed-loop pole configuration of the continuous system. As long as the closed-loop poles are located in the region of Fig. 9, the digital control system with a delay corresponding to system (8) is stable. Transforming the design of digital controllers into closed-loop pole configurations for continuous systems allows the design of digital controllers to be easily combined with other continuous controller design methods, such as robust control, through the LMI method.

For the convenience of understanding and design, the time-delay-stable closed-loop pole region design process is summarized in Fig. 10. Fig. 10. means to set an initial value $r = r_{int}$ first, obtain $\overline{t_{di}}(\theta = 0)$ through (20), and then iterate until r_s is obtained so that $t_d \approx \overline{t_{di}}(\theta = 0)$. Then, a point $\theta = \theta_s$ that satisfies $\overline{t_{di}}(\theta = \theta_s) = \overline{t_{di}}(\theta = 0)$ is obtained through a similar

process so that (19) has approximately the same solution. Finally, determine the closed area.

B. DESIGN OF A ROBUST LQR CONTINUOUS CONTROLLER

Another purpose of this article is to ensure the stability of the system in the presence of parameter uncertainty, which is why the designed controller is called robust.

The LMI method is suitable for addressing this kind of robust continuous control problem. Before the analysis and design, an important lemma is presented.

Lemma: Schur complementary lemma:

The following two equations are equivalent:

$$\begin{bmatrix} A_{11} & A_{12} \\ A_{21} & A_{22} \end{bmatrix} < 0 \Leftrightarrow \begin{cases} A_{22} < 0 \\ A_{11} - A_{12}A_{22}^{-1}A_{21} < 0 \end{cases} \tag{21}$$

For the continuous-time system described in (9), achieving the optimal output and dynamic response corresponds to minimizing the indicator function expressed as:

$$J(x,u) = \int_0^\infty x^T Qx + u^T Rudt \tag{22}$$

where Q and R are weighting matrices. According to [14], obtaining a solution that minimizes (22) is equivalent to solving the following LMIs at $P > 0, r > 0$:

$$\begin{cases} \min r \\ (AP + BW) + (AP + BW)^T + x_0^T x_0 < 0 \\ tr\left(Q^{1/2}P\left(Q^{1/2}\right)^T\right) + tr(Y) < r \\ \begin{bmatrix} -Y & R^{1/2}W \\ \left(R^{1/2}W\right)^T & -P \end{bmatrix} < 0 \end{cases} \tag{23}$$

where $W = KP$ and x_0 represents the state initial conditions. Since the variations in the input voltage, inductance, and capacitance are all upper bounded, the variations in the system matrices are also bounded. Taking matrix A as an example, if the upper bound of the change in each element of the matrix is defined as e_{ij}, then the current change of each element is $\Delta a_{ij} = h_{ij}f_{ij}e_{ij}$, where $h_{ij} = 1$ means that the current element is changed, $h_{ij} = 0$ indicates that there is no change, and $|f_{ij}| \le 1$ is the change rate. Then, the change in matrix A can be expressed as follows:

$$\Delta A = \begin{bmatrix} \Delta a_{11} & \Delta a_{12} \\ \Delta a_{21} & \Delta a_{22} \end{bmatrix} = \begin{bmatrix} h_{11}f_{11}e_{11} & h_{12}f_{12}e_{12} \\ h_{21}f_{21}e_{21} & h_{22}f_{22}e_{22} \end{bmatrix} = H_1F_1E_1 \tag{24}$$

where $H_1 = \begin{bmatrix} 1 & 0 \\ 0 & 1 \end{bmatrix}$, $E_1 = \begin{bmatrix} h_{11}e_{11} & h_{11}e_{12} \\ h_{11}e_{21} & h_{11}e_{22} \end{bmatrix}$, and $F_1 = \Delta A E_1^{-1}$. By definition, there must be $F^T F < I$. Therefore, the change in system parameters can be uniformly written in the form of a matrix as follows:

$$\begin{bmatrix} \Delta A & \Delta B \end{bmatrix} = HF\begin{bmatrix} E_1 & E_2 \end{bmatrix} \tag{25}$$

When there is parameter uncertainty, $AP + BW$ in (23) becomes $(A + \Delta A)P + (B + \Delta B)W$, and based on (25), the items containing parameter changes can be expressed as follows:

$$\Delta AP + \Delta BW = HF(E_1P + E_2W) \tag{26}$$

Since the matrix F represents parameter uncertainty and cannot be expressed by specific parameters, (26) cannot be directly brought into (23) for controller design. However, regardless of how F changes, there must be a square relationship greater than 0 as follows:

$$\left(\sqrt{\alpha}H^T - \sqrt{\alpha^{-1}}F\Psi\right)^T\left(\sqrt{\alpha}H^T - \sqrt{\alpha^{-1}}F\Psi\right) > 0 \tag{27}$$

where $\Psi = E_1P + E_2W$ and α is a constant satisfying $\alpha > 0$. Equation (27) can be expanded to obtain:

$$HF\Psi < \alpha HH^T + \alpha^{-1}\Psi^T F^T F\Psi \tag{28}$$

Since $F^T F < I$, (26) must be negative definite if and only if the following conditions are satisfied:

$$\alpha HH^T + \alpha^{-1}\Psi^T\Psi < 0 \tag{29}$$

Combined with the Schur complementary lemma and choosing $A_{11} = \Xi + \Xi^T + \alpha H^T H + x_0^T x_0$, $A_{21} = E_1P + E_2W$, $A_{12} = A_{21}^T$, and $A_{22} = -\alpha^{-1}$, (23) then becomes:

$$\begin{cases} \min r \\ \begin{bmatrix} \Xi + \Xi^T + x_0^T x_0 + \alpha H^T H & \Psi^T \\ \Psi & -\alpha I \end{bmatrix} < 0 \\ tr\left(Q^{1/2}P\left(Q^{1/2}\right)^T\right) + tr(Y) < r \\ \begin{bmatrix} -Y & R^{1/2}W \\ \left(R^{1/2}W\right)^T & -P \end{bmatrix} < 0 \end{cases} \tag{30}$$

where Ξ is $(AP + BW)$. The robust LQR continuous control rate of parameter variations of the system is $K = WP^{-1}$.

Thus, the LQR problem has been transformed into the form of an LMI, and parameter variations of the system are also considered.

However, this is a robust LQR problem for continuous-time systems, and the ultimate goal of this article is to design a robust LQR controller for digital systems.

C. DESIGN OF A ROBUST LQR DIGITAL CONTROLLER

According to the previous analysis, the design of a digital controller can be equivalent to the design of a continuous system with a time delay and then transformed into the problem of selecting the closed-loop pole region, which actually becomes the design of a digital controller in the continuous domain. Therefore, designing a robust LQR digital controller is equivalent to designing a robust LQR continuous controller within a specified closed-loop pole region. This can be expressed as follows:

$$D_{s\in DRL} = D_{s\in CRL} \cap D_{s\in D} \tag{31}$$

where $D_{s\in DRL}$ is the solution set of the robust LQR digital controller, $D_{s\in CRL}$ is the solution set of the robust LQR continuous controller, and $D_{s\in D}$ is the solution set of the delay-stabilized controller.

Since the design of the robust LQR continuous controller has been transformed into LMIs, if the closed-loop pole position of the robust LQR continuous controller is to be set in the region satisfying delay stability, then the closed-loop pole assignment problem must first be transformed into LMIs. If the configured pole region is symmetric about the real axis of the complex plane and is a convex region, then there exists $L_i \in \mathbb{S}^m$, $M_i \in \mathbb{R}^m$ such that the region can be expressed as:

$$\left\{s = x + yj | L_i + sM_i + \bar{s}M_i^T < 0\right\} \tag{32}$$

For the area enclosed by $-\beta \leq Re(\lambda) \leq -\alpha$ in Fig. 9, $L_1 = diag(2\alpha, -2\beta)$, and $M_1 = diag(1, -1)$. For the area enclosed by $r \leq r_s$ in Fig. 9, $L_2 = diag(-r_s, -r_s)$, and $M_2 = \begin{bmatrix} 0 & 1 \\ 0 & 0 \end{bmatrix}$. For the area enclosed by $-\theta_s \leq \theta \leq \theta_s$ in Fig. 9, $L_3 = 0$, and $M_3 = \begin{bmatrix} \sin\theta_s & \cos\theta_s \\ -\cos\theta_s & \sin\theta_s \end{bmatrix}$.

The closed-loop pole configuration in this region is equivalent to the existence of a positive definite matrix P such that the following expression holds:

$$L_i \otimes P + M_i \otimes (AP) + M_i^T \otimes (AP)^T < 0 \tag{33}$$

where $L_i \otimes P$ means each element of matrix L_i multiplied by P.

Based on the stability region obtained in Section III-A, combined with (30), the condition for delay stability of the system can be obtained according to the following matrix:

$$\begin{bmatrix} \Omega_1 & 0 & 0 \\ 0 & \Omega_2 & 0 \\ 0 & 0 & \Omega_3 \end{bmatrix} < 0 \tag{34}$$

where Ω_1, Ω_2, and Ω_3 are determined as:

$$\Omega_1 = \begin{bmatrix} 2\alpha P + \Xi + \Xi^T & 0 \\ 0 & -2\beta P - \Xi - \Xi^T \end{bmatrix}$$

$$\Omega_2 = \begin{bmatrix} -r_s P & \Xi \\ \Xi^T & -r_s P \end{bmatrix}$$

$$\Omega_3 = \begin{bmatrix} \sin\theta_s\left(\Xi + \Xi^T\right) & \cos\theta_s\left(\Xi - \Xi^T\right) \\ -\cos\theta_s\left(\Xi - \Xi^T\right) & \sin\theta_s\left(\Xi + \Xi^T\right) \end{bmatrix}$$

Due to the equivalence of the digital controller and the delay-stabilized controller, the gain matrix $[k_1\ k_2]$ of the robust LQR digital controller is obtained as the common solution of (30) and (34). Bringing $[k_1\ k_2]$ into (5) results in the final controller.

Thus, an LMI-based design method for a robust LQR digital controller is obtained. Although this form seems very complex, it is well suited for computer processing because the LMI problem can be transformed into a convex-optimal problem, which can actually greatly facilitate the design process.

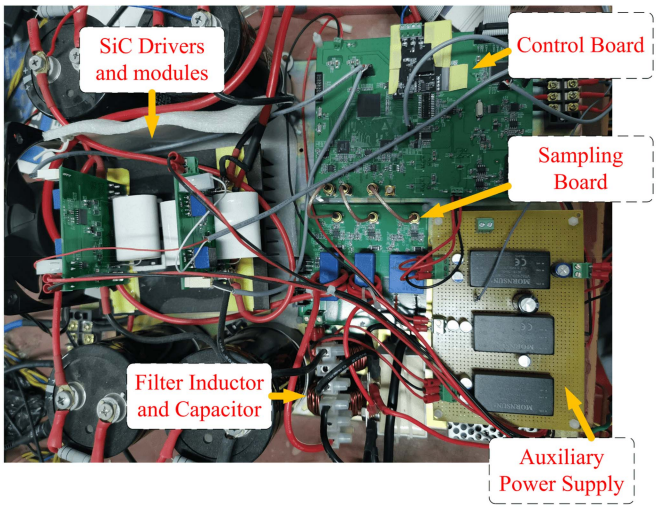

FIGURE 11. Experimental platform.

TABLE 2. Prototype Parameters

Parameters	Descriptions	Values	Units
V_{dc}	Input voltage	$500 \pm 8\%$	V
V_p	Positive output voltage	260	V
V_n	Negative output voltage	0	V
f_o	Output frequency	1000	Hz
C_o	Output capacitor	$2 \pm 10\%$	μF
L_f	Filter Inductance	$900 \pm 20\%$	μH
f_s	Switching frequency	200	kHz
t_{dead}	Dead time	200	ns
t_{sensor}	Sensor delay	3	μs
t_{SH-C}	Data conversion and calculation delay	1	μs
t_{PWM}	Max PWM delay	3.5	μs

IV. DESIGN EXAMPLES, ANALYSIS, SIMULATION AND EXPERIMENTAL VERIFICATION

A. DESIGN EXAMPLE, ANALYSIS AND SIMULATION COMPARISON

A prototype of the proposed robust LQR digital control is designed and implemented in the laboratory environment, as shown in Fig. 11, and the load is 30 Ω unless otherwise specified. The effectiveness and feasibility of the proposed control method are verified by experimental investigation. To demonstrate the control effects more clearly, the negative part of the output waveform is set to 0 V, which represents the worst case of output. The parameters and the delay time introduced by each stage are listed in Table 2. The controller chosen for the system is a Spartan6 from Xilinx.

The delay introduced by data conversion can be determined based on the clock frequency of the ADC and the number of clocks required for sampling, holding and conversion. Isolated voltage and current sensors usually have the Hall effect type and Σ-Δ type. The delay t_{sensor} introduced by the Hall effect type can be obtained from the datasheet, and the t_{sensor} of the Σ-Δtype can be calculated by using the digital filter structure and oversampling rate. The max PWM delay t_{pwm} can be

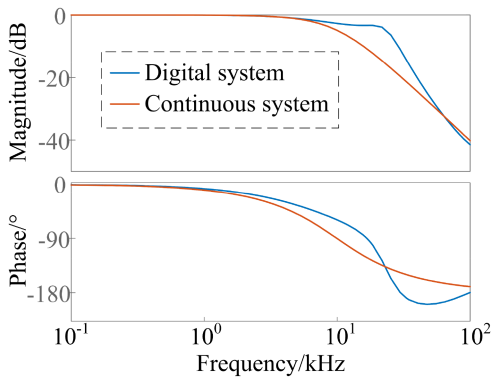

FIGURE 12. Bode plots of digital and continuous systems with $\mathcal{K}_1$.

calculated by the edge modulation mode and maximum duty cycle. Since the delay stability of the system is determined based on the delay upper bound, there is no need to know the precise delay value, only the maximum value. Therefore, if further assurance of stability is desired, margins can be considered.

Since the sum of the time delay introduced by each part of the system is 7.5 μs, according to the process in Fig. 10, $r_s = 86300$ and $\theta_s = 69\,^\circ$ can be derived as meeting the delay stability requirement of the closed-loop system. To limit the dynamic performance of the system, the parameters are chosen as $\theta_s = 60°$, $\alpha = 32000$, $\beta = 90000$, $Q = [10, 0; 0, 10]$, and $R = 10$. Since the variation range of the inductance is 720 μH $\le L_f \le$ 1080 μH, the maximum variation in $1/L_f$ is $1/(720\mu) - 1/(900\mu) = 278$. By analogy, combined with (23), $E_1 = \begin{bmatrix} 0 & 278 \\ 55555 & 0 \end{bmatrix}$ and $E_2 = \begin{bmatrix} 389000 & 0 \end{bmatrix}$ can be obtained.

The control law $\mathcal{K}_1$ is calculated as $[-0.0981 \quad -0.0060]$ by obtaining the common solution of (30) and (34). By solving (16), when the control law $\mathcal{K}_1$ is adopted, the maximum allowable delay for the closed-loop system is 11.2 μs when the system parameters are the rated values. Since the maximum time delay allowed by the system is greater than the actual time delay of the system, the system is stable. In addition, when the system parameters are $L = 720$ μH,$V_{dc} = 540$ V, and $C = 1.8$ μF, which is the worst case, the maximum allowable delay is obtained as 8.7 μs, which still satisfies the delay stability requirement.

Similar to (7), when the proposed digital control method is adopted, the approximate dynamic response of system (11) can also be analyzed by using the transfer function. Through a method similar to that for (7), the approximate transfer function from the reference signal u_{ref} to the output voltage u_o can be obtained as follows:

$$G_{ref-o} = \frac{(1 - 2k_2V_{dc})}{L_fC_fs^2 - 2C_fk_1V_{dc}e^{-t_ds}s + \left(1 - 2k_2V_{dc}e^{-t_ds}\right)} \tag{35}$$

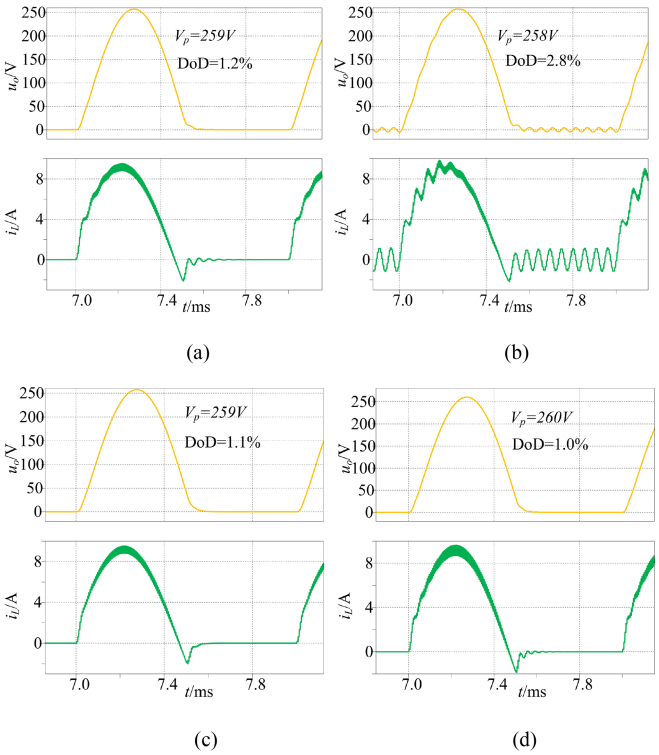

FIGURE 13. Inductor current and output voltage waveforms for different cases. (a) $t_d = 10.9$ μs and parameters are rated. (b) $t_d = 11.5$ μs and parameters are rated. (c) $t_d = 7.5$ μs and parameters are rated. (d) $t_d = 7.5$ μs and parameters are changed.

Fig. 12 shows the Bode plots of G_{ref-o} for digital control system (11) and continuous control system (9) when the control law $\mathcal{K}_1$ is used. Fig. 12 shows that whether it is a digital control system with a time delay or a continuous control system, the bandwidth of the closed-loop system is greater than 7.7 kHz, which can meet the output waveform quality requirements.

To verify the above analysis, a simulation using analog PWM modulation and no calculation delay was established, only adding delay in the sampling part to ensure the total delay. To identify the waveform quality of asymmetric sine waves, the degree of distortion (DoD) is introduced as an evaluation index as follows:

$$\mathrm{DoD} = \frac{\sqrt{\int_0^{T_o} \left(u_{ref} - u_o\right)^2 dt}}{\sqrt{\int_0^{T_o} u_{ref}^2 dt}} \times 100\% \tag{36}$$

where T_o is the period of the output waveform. A smaller DOD represents a smaller difference between the output waveform and the desired waveform, which means a higher quality.

Fig. 13(a) shows the output voltage waveform and inductor current waveform when there is no parameter change and the total delay is 10.9 μs. The system remains stable and the DoD is only 1.2%. In contrast, Fig. 13(b) shows the waveform when the total delay is 11.5 μs. Both the inductor current and output voltage waveforms show obvious oscillation, indicating that

the system is already unstable. This shows that the analysis of the maximum allowable delay of the system and the design method of the digital controller are correct.

Fig. 13(c) is the waveform when the total delay is 7.5 μs and there is no parameter change, and Fig. 13(d) is the waveform when the total delay is 7.5 μs but the parameters become $L = 720$ μH, $V_{dc} = 540$ V, and $C = 1.8$ μF. These changes come from bus voltage fluctuations, magnetic device saturation characteristics and manufacturing tolerances, and are manually added to the simulation to simulate the worst conditions. The systems are stable, which shows that the designed controllers have good robustness to parameter uncertainties.

To highlight the superiority of the proposed method, the effects of the general LQR control with error integral, repetitive control, MPC, SMC and deadbeat control are compared. When comparing the general LQR method, the selected state variable of the comparison system is $[i_L\ u_c\ \int(u_{ref} - u_c)dt]$, and a stable control law $\mathcal{K}_t = [0.223\ 0.027\ -595.616]$ under the delay $t_d = 7.5$ μs is obtained through debugging. Fig. 14(a) shows the output voltage waveform under rated parameters when using controller $\mathcal{K}_t$ with a delay of 7.5 μs. Due to the limited integral gain, the output impedance is large at high frequencies and the output amplitude is only 250 V, so the DoD is 5.9%. Fig. 14(b) shows the output voltage waveform when the parameter changes to $L = 720$ μH, $V_{dc} = 540$ V, and $C = 1.8$ μF, and the system is obviously unstable. Therefore, the existing general LQR control methods are inferior to the proposed method in terms of output waveform quality, load regulation rate, and stability.

Fig. 14(c) is the output voltage waveform when the repetitive controller is used and the extra time delay is 0. The repeat controller gain is 0.8 and the lead correction part is z^{10}. Additionally, since the amplitude is only 250 V, the DoD is 5.7%. Fig. 14(d) is the output voltage waveform when only 2 μs extra delay is added under repeated control, and the system is obviously unstable at this time. Systems using repetitive controls are less tolerant to delays than the proposed method.

Fig. 14(e) is the MPC. Since the MPC does not directly generate the duty cycle, to ensure the output ripple, the control cycle is selected as 1 μs, which is difficult to achieve in practice. Since the control frequency is much higher than other methods, the output waveform quality is very good, with a DoD of only 0.5%. However, as shown in Fig. 14(f), the system is already unstable with only 1μs of extra delay.

Fig. 14(g) shows the second-order SMC based on equivalent control theory, and the control variable is $[u_{ref} - u_o\ d(u_{ref} - u_o)/dt\ \ \int(u_{ref} - u_o)dt]$. Due to the differential term of the error, there is obvious jitter in the output waveform affected by noise. Fig. 14(h) shows that when the delay is also 7.5 μs, the sliding mode control becomes unstable, and the delay stability is worse than that of the proposed method.

Fig. 14(i) shows the deadbeat control, which also has good control performance under ideal conditions. However, since deadbeat control is highly dependent on the model, a delay

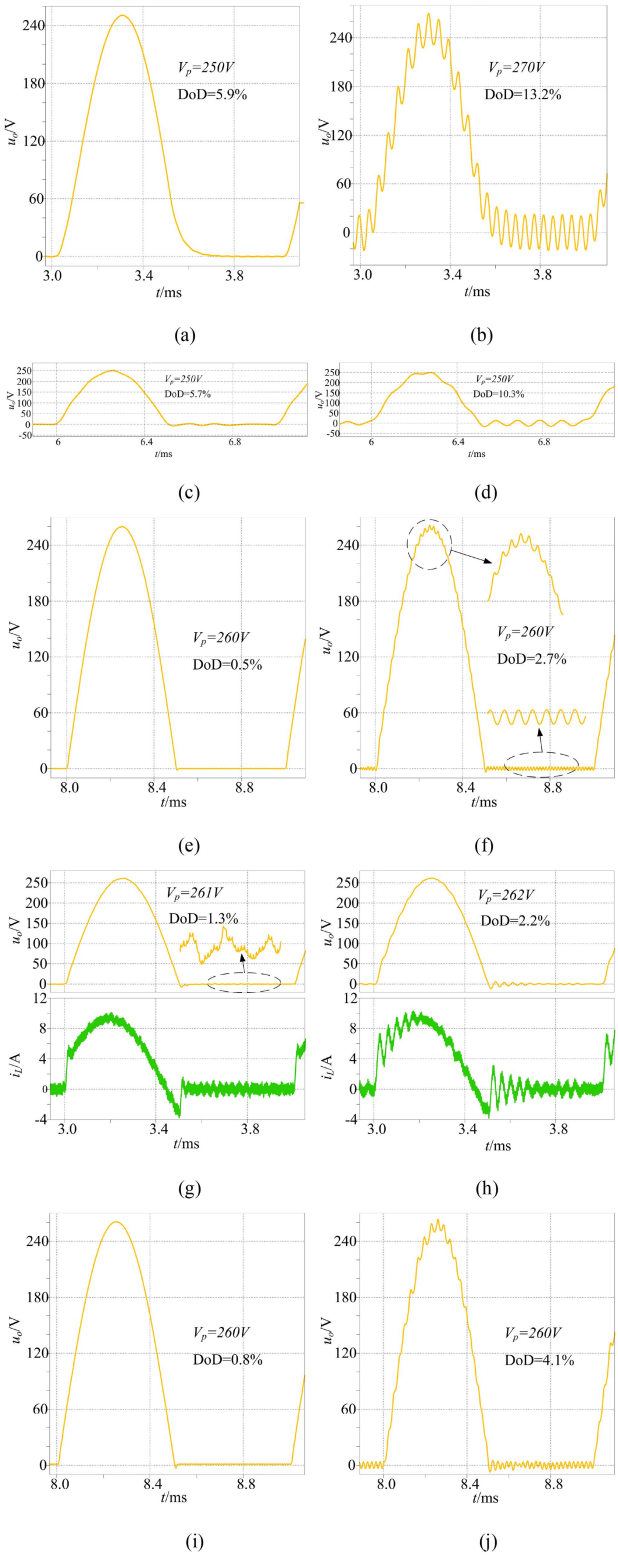

FIGURE 14. Output waveforms under different control methods and delays. (a) General LQR with 7.5 μs delay and rated parameters. (b) General LQR with 7.5 μs delay and changed parameters. (c) Repetitive control with 0 μs delay. (d) Repetitive control with 2 μs delay. (e) MPC with 0 μs delay. (f) MPC with 1 μs delay. (g) SMC with 0 μs delay. (h) SMC with 7.5 μs delay. (i) Deadbeat control with 0 μs delay. (j) Deadbeat control with 1 μs delay.

TABLE 3. Performance Comparison of Different Control Methods

Control methods	DoD with delay	Stability at 7.5 μs delay
Proposed method	1.1% with 7.5 μs	Stability
General LQR	13.2% with 7.5 μs	Instability
Repetitive control	10.3% with 2 μs	Instability
Model predictive control	2.7% with 1 μs	Instability
sliding-mode control	2.2% with 7.5 μs	Instability
Deadbeat control	4.1% with 1 μs	Instability

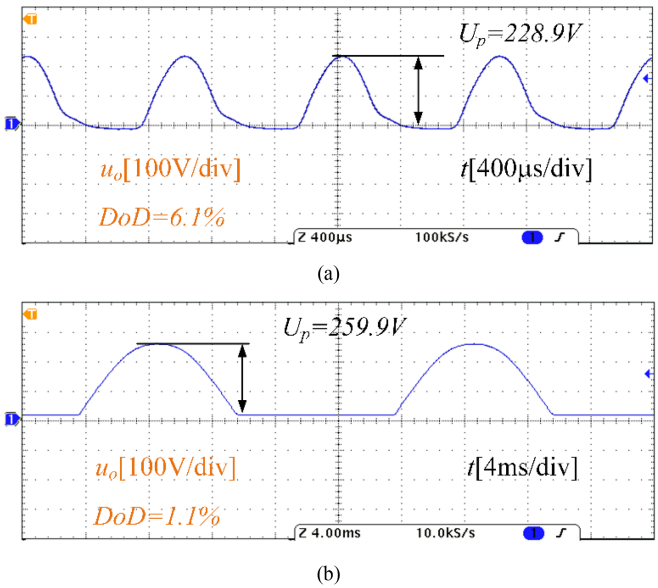

FIGURE 15. Output waveform under traditional PI control at different output frequencies: (a) 1 kHz. (b) 50 Hz.

of only 1 μs will make the system unstable, as shown in Fig. 14(j), and parameter changes will also lead to instability.

The simulation comparison results are summarized in Table 3. Compared with the existing typical control methods, the proposed method has better robustness to time delay and parameter uncertainty and stronger system stability while ensuring the output waveform quality and load regulation rate. In addition, the proposed method has predictable delay stability and a simpler implementation form, which is more conducive to application.

B. EXPERIMENTAL VERIFICATION

To further illustrate the necessity of using the proposed method, first, the experimental waveform of the output under traditional double closed-loop PI control is compared as shown in Fig. 15. Fig. 15(a) shows that when the output frequency is 1 kHz, the output waveform distortion is serious, and the amplitude of the output waveform cannot reach the rated value. However, Fig. 15(b) shows that at an output frequency of 50 Hz, the output waveform can achieve the required waveform quality. This is due to the additional delay in the actual system, and the traditional double closed-loop PI control needs to reduce the bandwidth to ensure stability. Therefore, it is difficult to guarantee the waveform quality of asymmetric sinusoidal waveforms.

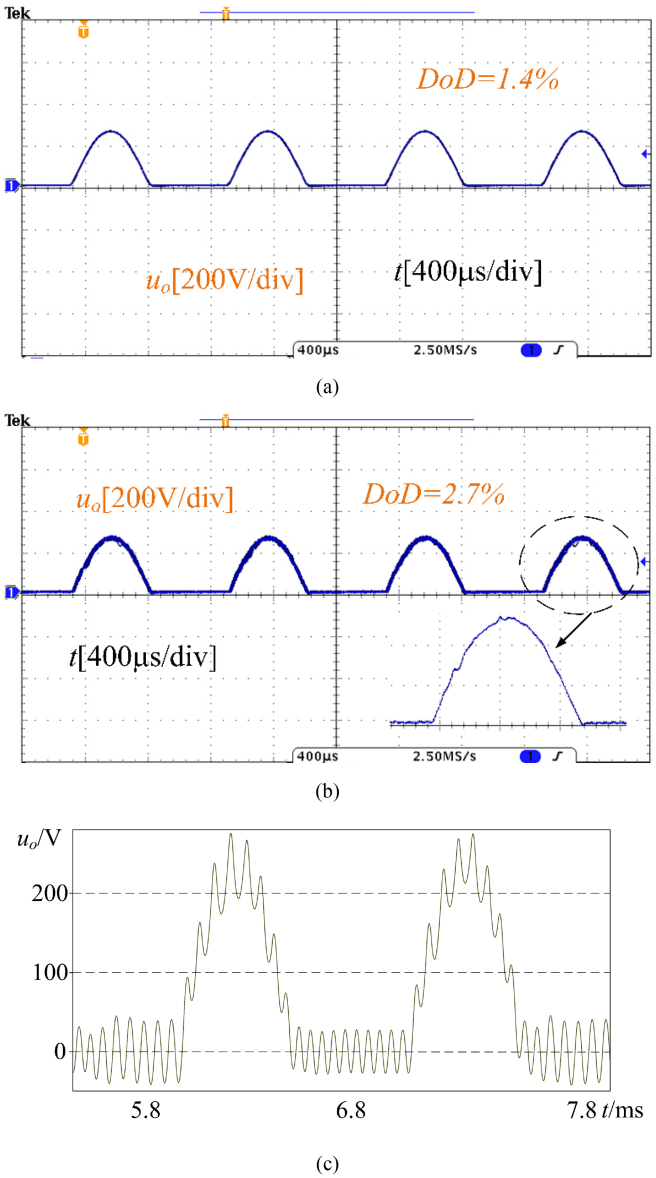

FIGURE 16. Comparison of output waveforms under different controllers (i.e., different maximum allowable time delay). (a) $\mathcal{K}_1$ (11.2 μs). (b) $\mathcal{K}_2$ (6.6 μs). (c) $\mathcal{K}_3$ (3.5 μs) (simulation).

As a comparison, Fig. 16 shows the output waveform when the proposed robust LQR digital control method is adopted. To further verify the correctness of the theory, a controller $\mathcal{K}_2 = [-0.1408 \quad -0.0217]$ with a maximum allowable delay of 6.6 μs is designed for comparison. Fig. 16(a) shows the output waveform when controller $\mathcal{K}_1$ is used. Similarly, Fig. 16(b) shows the output waveform when controller $\mathcal{K}_2$ is used. The oscillation in Fig. 16(b) indicates that the system has become unstable; the output waveform can still maintain the shape of an asymmetrical half-sine wave only due to the feed-forward signal u_f, and the DoD at this time is 2.7%. In contrast, Fig. 16(a) shows that the output waveform quality of the system is good, and the DoD is as low as 1.4%, which also shows that the system is stable. Furthermore, the controller

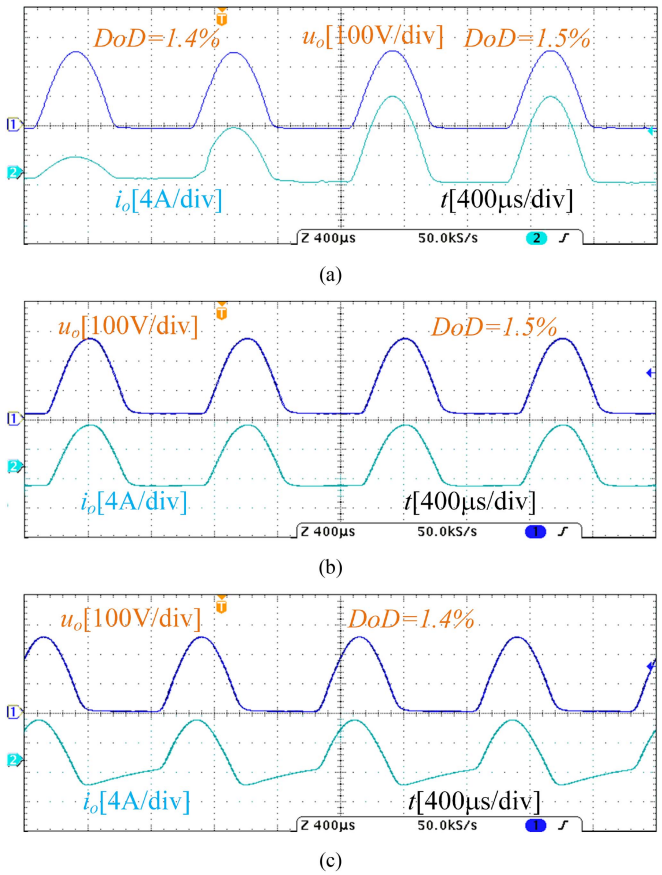

FIGURE 17. Output waveforms under different loads using the proposed method. (a) 3-11A step load. (b) 30 Ω + 200 μH. (c) 30 Ω + 15 μF.

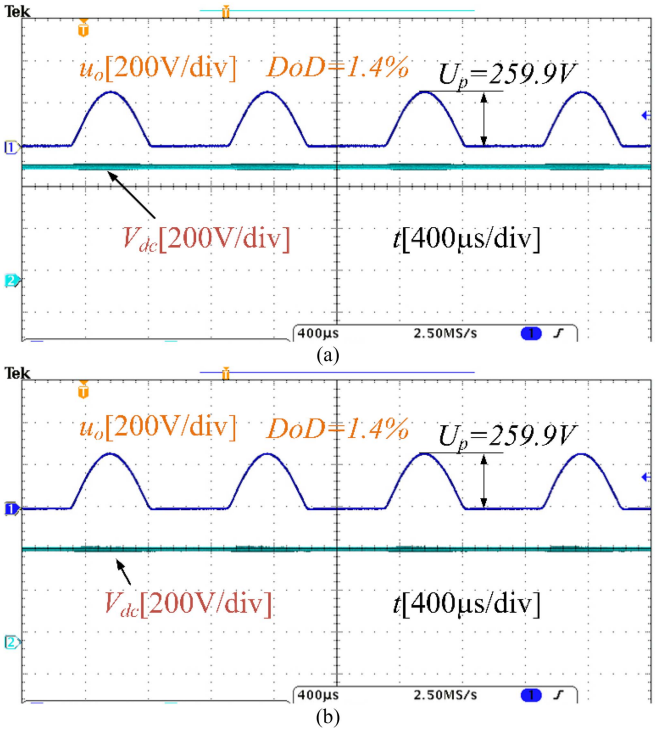

FIGURE 18. Input and output voltage waveforms at different input voltages: (a) 540 V. (b) 460 V.

$\mathcal{K}_3 = [-0.2762 \quad -0.0774]$ designed by the traditional LQR digital control design method using the MATLAB dlqr function is also verified, but because the controller $\mathcal{K}_3$ makes the maximum allowable delay of the system only 3.5 μs, the system is completely unstable, which will trigger protection in the experiment; thus, the simulation waveform is used as a substitute, as shown in Fig. 16(c). Fig. 16(c) shows that when the system has a time delay, the traditional digital control design method does not necessarily guarantee stability.

The output waveforms under different load conditions are also tested to verify the effectiveness of the proposed control method. Fig. 17(a) shows the output voltage and current waveforms when the resistive load is stepped from 3 A to 11 A. Fig. 17(b) shows the situation of simulating a long line with a resistive load, that is, a resistive series inductive load, and the test condition is 30 Ω+200 μH. Fig. 17(c) shows the situation of simulating a microarc oxidation load, which is simplified as a resistive series capacitive load, and the test condition is 30 Ω+15 μF. Fig. 17 shows that when using the proposed control method, the system can maintain stability under different load conditions, and the system always has high waveform quality and load regulation.

The robustness of the proposed control method to parameter uncertainties is also verified, first, for the bus voltage. Fig. 18 shows the output voltage and input voltage waveforms when the input voltage changes. When the input voltage changes from 460 V to 540 V, the system is not only stable but also maintains the output waveform quality. This indicates that the designed controller can suppress the effect of input voltage changes and has good robustness to the input voltage. In addition, since the feed-forward information of the input voltage is introduced in the control, the influence of changes in the input voltage on the output waveform is also suppressed.

Fig. 19 shows the output voltage waveform when the filter capacitance is varied by ±10%, which meets the specifications of most film capacitors. The system shows a stable response and presents a high waveform quality when the filter capacitance is varied. Due to the magnetic material, the designed inductor itself changes inductance when the load current changes, and no additional verification is needed. Fig. 17(a) shows that the system is stable when the inductor parameters change. The waveforms in Figs. 17, 18, and 19 demonstrate the robustness of the designed controller to system parameter variations or uncertainties.

In addition, to further verify that the proposed method is indeed robust to parameter uncertainties, a controller $\mathcal{K}_4 = [-0.1050 \quad -0.0124]$ that only satisfies delay stability (34) and not robustness (30) is designed for verification. Fig. 20 shows the output voltage waveform and inductor current waveform when the system is in the worst case, that is, $L = 720$ μH, $V_{dc} = 540$ V, and $C = 1.8$ μF. The inductor current in Fig. 20 begins to oscillate, indicating that the system is

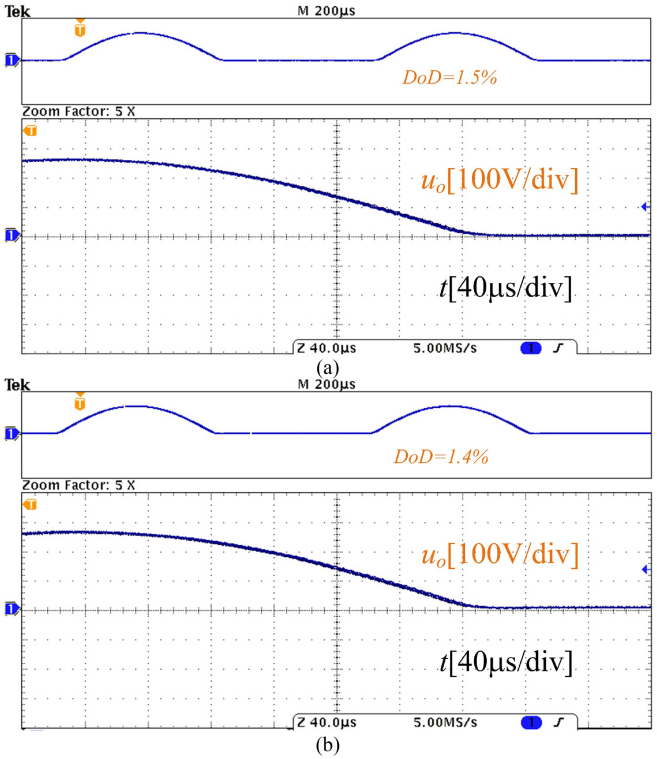

FIGURE 19. Output voltage and detailed zoomed-in waveforms at different filter capacitances: (a) 2.2 μF. (b) 1.8 μF.

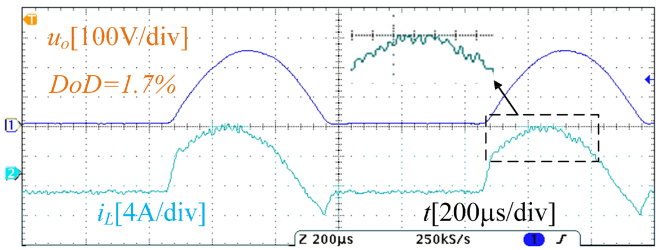

FIGURE 20. Output voltage and inductor current waveforms when using controller $\mathcal{K}_4$.

beginning to become unstable. Compared with experiments, the proposed method can ensure robustness to parameter uncertainty, but if the proposed method is not used, stability cannot be guaranteed when the parameters change.

V. CONCLUSION

In an asymmetric sinusoidal microarc oxidation inverter, the rich harmonics of the output waveform, parameter uncertainty, and delay introduced at each stage are challenges to the design of the controller, especially when the output frequency is higher. This article presents a novel robust LQR digital control method for high-bandwidth inverters. The proposed method ensures the output waveform by combining feedforward and state feedback and greatly simplifies the controller design difficulty by converting the design of the digital controller into a time domain pole configuration method, while allowing the system to include additional delays. In addition, robustness to parameter uncertainties is considered in the design of the digital controller.

Simulation and experiments show that compared with the existing control methods, the proposed method can guarantee the output waveform quality, load regulation and stability at the same time. The proposed method has predictable stability due to the consideration of delay and parameter uncertainty. In addition, because the proposed method is simple to implement, requires low computing power, and can achieve high bandwidth, it is especially suitable for inverters with high switching frequency and output frequency. However, the proposed method is a general method and can also be used for power factor correction and dc-dc converters.

At present, the proposed method still needs computer assistance to obtain a stable pole region when designing a digital controller with an extra delay. The next step will be to propose a simpler method for obtaining a stable region. In addition, the proposed method is suitable for fixed switching frequency systems, and the next research goal is to extend it to variable frequency systems such as CRM inverters.

REFERENCES

[1] L. R. Krishna, K. Somaraju, and G. Sundararajan, "The tribological performance of ultra-hard ceramic composite coatings obtained through microarc oxidation," *Surf. Coatings Technol.*, vol. 163, pp. 484–490, Jan. 2003.

[2] J. L. Lee, S. Y. Jian, K. N. Kuo, J. L. You, and Y. T. Lai, "Effect of surface properties on corrosion resistance of ZK60 Mg alloy microarc oxidation coating," *IEEE Trans. Plasma Sci.*, vol. 47, no. 2, pp. 1172–1180, Feb. 2019.

[3] M. Chen, M. A. Yuezhou, and Y. Hao, "Local arc discharge mechanism and requirements of power supply in micro-arc oxidation of magnesium alloy," *Front. Mech. Eng.*, vol. 5, no. 1, pp. 98–105, 2010.

[4] J. Andino, P. Ayala, J. Llanos-Proaño, D. Naunay, W. Martinez, and D. Arcos-Aviles, "Constrained modulated model predictive control for a three-phase three-level voltage source inverter," *IEEE Access*, vol. 10, pp. 10673–10687, 2022.

[5] N. Guler and H. Komurcugil, "Energy function based finite control set predictive control strategy for single-phase split source inverters," *IEEE Trans. Ind. Electron.*, vol. 69, no. 6, pp. 5669–5679, Jun. 2022.

[6] P. Mattavelli, "An improved deadbeat control for UPS using disturbance observers," *IEEE Trans. Ind. Electron.*, vol. 52, no. 1, pp. 206–212, Feb. 2005.

[7] A. Lidozzi, C. Ji, L. Solero, P. Zanchetta, and F. Crescimbini, "Digital deadbeat and repetitive combined control for a stand-alone four-leg VSI," *IEEE Trans. Ind. Appl.*, vol. 53, no. 6, pp. 5624–5633, Nov./Dec. 2017.

[8] K. Seifi and M. Moallem, "An adaptive PR controller for synchronizing grid-connected inverters," *IEEE Trans. Ind. Electron.*, vol. 66, no. 3, pp. 2034–2043, Mar. 2019.

[9] S.-L. Jung and Y.-Y. Tzou, "Discrete sliding-mode control of a PWM inverter for sinusoidal output waveform synthesis with optimal sliding curve," *IEEE Trans. Power Electron.*, vol. 11, no. 4, pp. 567–577, Jul. 1996.

[10] M. Xue, Y. Zhang, Y. Kang, Y. Yi, S. Li, and F. Liu, "Full feedforward of grid voltage for discrete state feedback controlled grid-connected inverter with LCL filter," *IEEE Trans. Power Electron.*, vol. 27, no. 10, pp. 4234–4247, Oct. 2012.

[11] J. Liu, Y. Miura, and T. Ise, "Fixed-parameter damping methods of virtual synchronous generator control using state feedback," *IEEE Access*, vol. 7, pp. 99177–99190, 2019.

[12] X. Bao, F. Zhuo, Y. Tian, and P. Tan, "Simplified feedback linearization control of three-phase photovoltaic inverter with an LCL filter," *IEEE Trans. Power Electron.*, vol. 28, no. 6, pp. 2739–2752, Jun. 2013.

[13] C. A. Busada, S. G. Jorge, and J. A. Solsona, "Full-state feedback equivalent controller for active damping in LCL-filtered grid-connected inverters using a reduced number of sensors," *IEEE Trans. Ind. Electron.*, vol. 62, no. 10, pp. 5993–6002, Oct. 2015.
[14] C. Olalla, R. Leyva, A. E. Aroudi, and I. Queinnec, "Robust LQR control for PWM converters: An LMI approach," *IEEE Trans. Ind. Electron.*, vol. 56, no. 7, pp. 2548–2558, Jul. 2009.
[15] N. Arab, H. Vahedi, and K. Al-Haddad, "LQR control of single-phase grid-tied PUC5 inverter with LCL filter," *IEEE Trans. Ind. Electron.*, vol. 67, no. 1, pp. 297–307, Jan. 2020, doi: 10.1109/TIE.2019.2897544.
[16] B. Kedjar and K. Al-Haddad, "DSP-based implementation of an LQR with integral action for a three-phase three-wire shunt active power filter," *IEEE Trans. Ind. Electron.*, vol. 56, no. 8, pp. 2821–2828, Aug. 2009, doi: 10.1109/TIE.2008.2006027.
[17] C. Chen, J. Xiong, Z. Wan, J. Lei, and K. Zhang, "A time delay compensation method based on area equivalence for active damping of an LCL -type converter," *IEEE Trans. Power Electron.*, vol. 32, no. 1, pp. 762–772, Jan. 2017, doi: 10.1109/TPEL.2016.2531183.
[18] O. J. M. Smith, "Closer control of loops with dead time," *Chem. Eng. Prog.*, vol. 53, no. 5, pp. 217–219, Jan. 1957.
[19] V. Miskovic, V. Blasko, T. M. Jahns, A. H. C. Smith, and C. Romenesko, "Observer-based active damping of LCL resonance in grid-connected voltage source converters," *IEEE Trans. Ind. Appl.*, vol. 50, no. 6, pp. 3977–3985, Nov./Dec. 2014, doi: 10.1109/TIA.2014.2317849.
[20] S. Bibian and H. Jin, "High performance predictive dead-beat digital controller for DC power supplies," *IEEE Trans. Power Electron.*, vol. 17, no. 3, pp. 420–427, May 2002, doi: 10.1109/TPEL.2002.1004250.
[21] S. Bibian and H. Jin, "Time delay compensation of digital control for DC switchmode power supplies using prediction techniques," *IEEE Trans. Power Electron.*, vol. 15, no. 5, pp. 835–842, Sep. 2000, doi: 10.1109/63.867672.
[22] G. Ripamonti et al., "A dual-edge pulsewidth modulator for fast dynamic response DC–DC converters," *IEEE Trans. Power Electron.*, vol. 34, no. 1, pp. 28–32, Jan. 2019, doi: 10.1109/TPEL.2018.2836385.
[23] H. Deng, R. Oruganti, and D. Srinivasan, "PWM methods to handle time delay in digital control of a UPS inverter," *IEEE Power Electron. Lett.*, vol. 3, no. 1, pp. 1–6, Mar. 2005, doi: 10.1109/LPEL.2004.842402.
[24] D. Pan, X. Ruan, C. Bao, W. Li, and X. Wang, "Capacitor-current-feedback active damping with reduced computation delay for improving robustness of LCL-type grid-connected inverter," *IEEE Trans. Power Electron.*, vol. 29, no. 7, pp. 3414–3427, Jul. 2014, doi: 10.1109/TPEL.2013.2279206.
[25] Z. Xin, X. Wang, P. C. Loh, and F. Blaabjerg, "Grid-current-feedback control for LCL-filtered grid converters with enhanced stability," *IEEE Trans. Power Electron.*, vol. 32, no. 4, pp. 3216–3228, Apr. 2017, doi: 10.1109/TPEL.2016.2580543.
[26] S. Prakash, J. K. Singh, R. K. Behera, and A. Mondal, "A type-3 modified SOGI-PLL with grid disturbance rejection capability for single-phase grid-tied converters," *IEEE Trans. Ind. Appl.*, vol. 57, no. 4, pp. 4242–4252, Jul./Aug. 2021, doi: 10.1109/TIA.2021.3079122.
[27] A. Ingimundarson and T. Hagglund, "Robust tuning procedures of dead-time compensating controllers," *Control Eng. Pract.*, vol. 9, no. 11, pp. 1195–1208, Nov. 2001.
[28] T. Liu, P. García, Y. Chen, X. Ren, P. Albertos, and R. Sanz, "New predictor and 2DOF control scheme for industrial processes with long time delay," *IEEE Trans. Ind. Electron.*, vol. 65, no. 5, pp. 4247–4256, May 2018.
[29] Q. L. Han, "Absolute stability of time-delay systems with sector-bounded nonlinearity," *Automatica*, vol. 41, no. 12, pp. 2171–2176, Dec. 2005.
[30] Z. Wei and Y. Ma, "Robust H-infinity observer-based sliding mode control for uncertain Takagi-Sugeno fuzzy descriptor systems with unmeasurable premise variables and time-varying delay," *Inf. Sci.*, vol. 566, pp. 239–261, Aug. 2021.
[31] D. Zhang and Y. Li, "Survey on the stability analysis of linear time-delay systems," *Control Decis.*, vol. 23, no. 8, pp. 841–849, Aug. 2008.
[32] Y. He, M. Wu, J. H. She, and G. P. Liu, "Parameter-dependent Lyapunov functional for stability of time-delay systems with polytopic-type uncertainties," *IEEE Trans. Autom. Control*, vol. 49, no. 5, pp. 828–832, May 2004.
[33] E. Fridman, A. Seuret, and J. P. Richard, "Robust sampled-data stabilization of linear systems: An input delay approach," *Automatica*, vol. 40, no. 8, pp. 1441–1446, Aug. 2004.
[34] M. Lu, A. Al-Durra, S. M. Muyeen, S. Leng, P. C. Loh, and F. Blaabjerg, "Benchmarking of stability and robustness against grid impedance variation for LCL -filtered grid-interfacing inverters," *IEEE Trans. Power Electron.*, vol. 33, no. 10, pp. 9033–9046, Oct. 2018.
[35] Y. He, X. Wang, X. Ruan, D. Pan, and K. Qin, "Hybrid active damping combining capacitor current feedback and point of common coupling voltage feedforward for LCL-type grid-connected inverter," *IEEE Trans. Power Electron.*, vol. 36, no. 2, pp. 2373–2383, Feb. 2021.
[36] J. Kim, H. H. Choi, and J. W. Jung, "MRAC-based voltage controller for three-phase CVCF inverters to attenuate parameter uncertainties under critical load conditions," *IEEE Trans. Power Electron.*, vol. 35, no. 1, pp. 1002–1016, Jan. 2020.
[37] S. A. Q. Mohammed, M. S. Rafaq, H. H. Choi, and J. W. Jung, "A robust adaptive PI voltage controller to eliminate impact of disturbances and distorted model parameters for 3-phase CVCF inverters," *IEEE Trans. Ind. Informat.*, vol. 16, no. 4, pp. 2168–2176, Apr. 2020.
[38] C. R. D. Osório, G. G. Koch, H. Pinheiro, R. C. L. F. Oliveira, and V. F. Montagner, "Robust current control of grid-tied inverters affected by LCL filter soft-saturation," *IEEE Trans. Ind. Electron.*, vol. 67, no. 8, pp. 6550–6561, Aug. 2020.
[39] L. A. Maccari et al., "LMI-based control for grid-connected converters with LCL filters under uncertain parameters," *IEEE Trans. Power Electron.*, vol. 29, no. 7, pp. 3776–3785, Jul. 2014.
[40] L. Huang, H. Xin, and F. Dörfler, "H∞-control of grid-connected converters: Design, objectives and decentralized stability certificates," *IEEE Trans. Smart Grid*, vol. 11, no. 5, pp. 3805–3816, Sep. 2020.
[41] Z. Li, C. Zang, P. Zeng, H. Yu, S. Li, and J. Bian, "Control of a grid-forming inverter based on sliding-mode and mixed H-2/H-infinity control," *IEEE Trans. Ind. Electron.*, vol. 64, no. 5, pp. 3862–3872, May 2017.
[42] S. Yang, Q. Lei, F. Z. Peng, and Z. Qian, "A robust control scheme for grid-connected voltage-source inverters," *IEEE Trans. Ind. Electron.*, vol. 58, no. 1, pp. 202–212, Jan. 2011.
[43] D. O. Neacşu and A. Sîrbu, "Design of a LQR-based boost converter controller for energy savings," *IEEE Trans. Ind. Electron.*, vol. 67, no. 7, pp. 5379–5388, Jul. 2020, doi: 10.1109/TIE.2019.2934062.
[44] P. M. de Almeida et al., "Systematic design of a DLQR applied to grid-forming converters," *IEEE J. Emerg. Sel. Topics Ind. Electron.*, vol. 1, no. 2, pp. 200–210, Oct. 2020, doi: 10.1109/JESTIE.2020.3017124.
[45] J. E. Courtois and P. Delrieu, "The use of models with aftereffect in problems of the design of optimal digital control systems," *Avtomatika i Telemekhanika*, vol. 16, no. 1/2, pp. 55–60, 1992.
[46] K. Gopalsamy, *Stability and Oscillations in Delay Differential Equations of Population Dynamics*. Berlin, Germany: Springer, 1992.

JICHAO NING was born in Inner Mongolia Province, China, in 1995. He received the B.S. degree in electrical engineering from the Xi'an University of Science and Technology, Xi'an, China, in 2016. He is currently working toward the Ph.D. degree in electrical engineering with the Harbin Institute of Technology, Harbin, China. His research interests include special power supply, converter modulation techniques, and advanced control techniques.

HONGQI BEN was born in Heilongjiang, China, in 1965. He received the B.S. degree in electrical engineering from the Shenyang University of Technology, Shenyang, China, in 1988, the M.S. degree in electrical engineering, and the Ph.D. degree in mechanical engineering from the Harbin Institute of Technology, Harbin, China, in 1991 and 1999, respectively. He is currently a Professor with the School of Electrical Engineering and Automation, Harbin Institute of Technology. His research interests include high frequency conversion and power factor correction techniques.

XUESONG WANG was born in Heilongjiang Province, China. He received the Ph.D. degrees in electrical engineering from the Harbin Institute of Technology, Harbin, China, in 2020. He is currently an Engineer with State Grid Harbin Power Supply Company. His research interests include power factor correction techniques, power quality, and distributed renewables.

TAO MENG (Member, IEEE) was born in Liaoning Province, China, in 1980. He received the B.S., M.S., and Ph.D. degrees in electrical engineering from the Harbin Institute of Technology, Harbin, China, in 2003, 2005, and 2010, respectively. He is currently a Professor with the School of Mechanical and Electrical Engineering, Heilongjiang University, Harbin. His research interests include high frequency ac/dc and dc/dc conversion, high frequency magnetic device, and power factor correction techniques